



Mixing-layer-height-referenced ozone vertical distribution in the lower troposphere of Chinese megacities: Stratification, classification, meteorological, and photochemical mechanisms

Zhiheng Liao^{a, b}, Meng Gao^c, Jinqiang Zhang^{d, e}, Jiaren Sun^f, Jiannong Quan^a, Xingcan Jia^a, Yubing Pan^a, Shaojia Fan^{b, g}

5

^a Institute of Urban Meteorology, Chinese Meteorological Administration, Beijing, China

^b School of Atmospheric Sciences, Sun Yat-Sen University, Zhuhai, China

^c Department of Geography, Hong Kong Baptist University, Hong Kong SAR, China

^d Key Laboratory of Middle Atmosphere and Global Environment Observation, Institute of Atmospheric Physics,
10 Chinese Academy of Sciences, Beijing, China

^e College of Earth and Planetary Sciences, University of Chinese Academy of Sciences, Beijing 100049, China

^f Key Laboratory of Urban Ecological Environmental Simulation and Protection of Ministry of Environmental
Protection, South China Institute of Environmental Sciences, Ministry of Ecology and Environment of the PRC,
Guangzhou, China

^g Guangdong Provincial Observation and Research Station for Climate Environment and Air Quality Change in the
15 Pearl River Estuary, Key Laboratory of Tropical Atmosphere–Ocean System, Ministry of Education, Southern
Marine Science and Engineering Guangdong Laboratory (Zhuhai), Zhuhai, China

Corresponding author: S. J. Fan (eesfsj@mail.sysu.edu.cn)

20 **Abstract:** Traditional tropospheric ozone (O_3) climatology uses a simple average substantially smoothed
stratification structure in individual O_3 profiles, limiting our ability to properly describe and understand how O_3 is
vertically distributed at the interface between the mixing layer (ML) and free troposphere (FT). In this study, we
collected 1,897 ozonesonde profiles from two Chinese megacities (Beijing and Hong Kong) over the period 2000–
2022 to investigate climatological vertical heterogeneity of lower-tropospheric O_3 distribution with a
25 mixing-layer-height-referenced (h -referenced) vertical coordinate system. The mixing layer height (h) was first
estimated following an integral method that integrates the information of temperature, humidity, and cloud. After
that, a so-called h -referenced vertical distribution of O_3 was determined by averaging all individual profiles
expressed as a function of z/h rather than z (where z is altitude). We found that the vertical stratification of O_3 is
distributed heterogeneously in the lower troposphere, with stronger vertical gradients at the surface layer and ML–
30 FT interface. There are low vertical autocorrelations of O_3 between the ML and FT, but high autocorrelations within
each of the two atmospheric compartments. These results suggest that the ML–FT interface acts as a geophysical
“barrier” separating air masses of distinct O_3 loadings. This barrier effect varies with season and city, with an
ML-to-FT detrainment barrier in summer (autumn) and an FT-to-ML entrainment barrier in other seasons in Beijing
(Hong Kong). Based on Student’s t test, h -referenced O_3 profiles were further classified into three typical patterns:
35 MLO₃-dominated, FTO₃-dominated, and uniform distribution. Although the FTO₃-dominated pattern occurs most
frequently during the whole study period (69% and 54% of days in Beijing and Hong Kong, respectively), the
MLO₃-dominated pattern prevails in the photochemical active season, accounting for 47% of summer days in
Beijing and 54% of autumn days in Hong Kong. These occurrences of the MLO₃-dominated pattern are
significantly more frequent than in previously reported results at northern mid-latitudes, indicating intensive
40 photochemical MLO₃ production under the high-emission background of Chinese megacity. From FTO₃-dominated
to MLO₃-dominated pattern, the O_3 precursor CH₂O (NO₂) experiences a substantial increase (decrease) in Beijing,



but a slight increase (decrease) in Hong Kong. Vertically, the increment of CH₂O is larger in the upper ML and the decrement of NO₂ is larger in the lower ML. Such changes in O₃ precursors push O₃ production sensitivity away from the VOC-limited regime and facilitate high-efficiency production of O₃ via photochemical reactions, particularly in the upper ML.

1 Introduction

Ozone (O₃), the dominant precursor of hydroxyl radicals, plays a crucial role in tropospheric chemistry. It is also an important greenhouse gas closely related to climate change and environmental issues (Seinfeld and Pandis, 2016; Monks et al., 2015). Being an air pollutant, O₃ can influence air quality on a hemispheric scale, exerting detrimental effects on human health and vegetation (Fleming et al., 2018; Mills et al., 2018). Tropospheric O₃ is primarily formed through a complex series of photochemical reactions between nitrogen oxides (NO_x) and volatile organic compounds (VOCs) in the presence of sunlight (Seinfeld and Pandis, 2016). There are substantial emissions of NO_x and VOCs in urban regions, where most of the population and industry are concentrated. As a result, elevated O₃ concentrations in the lower troposphere remain a persistent environmental problem in urban regions around the world (Lu et al., 2018). Significant efforts have been made to understand O₃ pollution in different cities (Monks et al., 2015). However, most previous studies were based on ground-based observations, and gave only limited insight into O₃ vertical distribution.

O₃ vertical distribution in the lower troposphere can provide very important information for mechanistic understanding of surface O₃ pollution (He et al., 2021; Lin et al., 2010; Jaffe, 2011; Yates et al., 2017). One of the major advantages when dealing with O₃ profile data is able to discriminate the two specific O₃ components corresponding to the two “reservoirs”—the mixing layer (ML) and the free troposphere (FT)—and therefore, to determine the direction and intensity of vertical exchange processes across the ML-FT interface. Several studies have been made trying to resolve the O₃ vertical exchange problem in the lower troposphere (Neuman et al., 2012; Berkes et al., 2016; Kaser et al., 2017; Trousdell et al., 2016; Zhao et al., 2019; Lin et al., 2010; Zhu et al., 2020). For example, based on tethered ozone soundings during a four-day ozone episode in southern Taiwan, Lin et al. (2010) revealed that the increase rate of surface O₃ concentration due to the downward mixing of the O₃ from the O₃ reservoir layers can be as high as 12–24 ppbv h⁻¹ in the late morning. Based on 214 aircraft vertical profiles in Colorado during summer 2014, Kaser et al. (2017) investigated the O₃ vertical gradient between the ML and the FT in order to estimate the FT-to-ML O₃ entrainment and to evaluate its representation in the WRF-Chem model. Their study focusing on the O₃ entrainment highlighted deficiencies in the model, indicating an overestimation of the O₃ entrainment and a too-efficient vertical mixing in the lower ML. These deficiencies were found to originate mainly from errors in the entrainment rate and ML height during the morning and an erroneous representation of the O₃ gradient at the ML-FT interface during the rest of the day. Overall, by measuring the specific terms in the vertical O₃ budget, detailed comparisons with photochemical models can uncover distinct weaknesses in current models and discern whether the difficulties lie in dynamical (transport) or chemical aspects of the numerical efforts (Trousdell et al., 2016).

O₃ vertical stratification below and above the ML-FT interface (i.e., the mixing layer height, *h*) is the basis for ozone vertical exchange processes. The formation of O₃ stratification is mainly due to the fact that the turbulent-convective ML and overlaying FT are usually separated by the mixing layer capping inversion, which acts as a transport barrier (Donnell et al., 2001). This barrier is indicated by steep vertical gradients of meteorological variables and chemical constituents (Petetin et al., 2018; Wyngaard and Brost, 1984; Williams et al., 2011). This means that climatological *h*-referenced O₃ vertical distribution in the lower troposphere could provide a useful



reference for understanding vertical exchange processes and validating air quality numerical models. However, tropospheric O₃ climatology is traditionally formed in a sea-level-referenced vertical coordinate system (Ding et al., 2008; Liao et al., 2021; Diab et al., 2004; Yonemura et al., 2002; Stauffer et al., 2016). Owing to day-to-day variation in the mixing layer top height, vertical stratification introduced in all individual profiles can be substantially smoothed in climatological profile when adopting the traditional vertical coordinate system. To address this issue, Petetin et al. (2018) proposed *h*-referenced climatology of lower-tropospheric O₃ profiles based on aircraft and ozonesondes at northern mid-latitudes over 1994–2016. When adopting this *h*-referenced vertical coordinate system, O₃ vertical stratification can be well preserved in lower-tropospheric O₃ climatology, demonstrating a significant improvement in capturing possible specific features (i.e., stratification) in the O₃ vertical distribution that would be smoothed with a simple average, in particular at the ML–FT interface. However, the *h*-referenced O₃ climatology in Petetin et al. (2018) is a hemispheric-scale composite result, which cannot represent the state over polluted urban regions, including megacities.

O₃ pollution has long been a significant environmental issue in China, despite the 2013 Clean Air Action Plan. In recent photochemical active seasons, O₃ overtook fine particles as the most important air pollutant in the three major city agglomerations: the North China Plain (NCP), the Yangtze River Delta (YRD), and the Pearl River Delta (PRD). As such, urban O₃ pollution is becoming a priority for scientific research and control strategies in China (Lu et al., 2018; Wang et al., 2022b), and numerous studies have explored the spatiotemporal characteristics and formation mechanisms of surface O₃ pollution, as summarized in Wang et al. (2017) and Wang et al. (2022b). Moreover, there are ongoing efforts to understand the role of vertical exchange in surface O₃ pollution in China based on vertical observations from tower-based, tethered-balloon-based, unmanned-aerial-vehicle-based, aircraft-based, and lidar-based observations (Lin et al., 2010; Zhao et al., 2019; He et al., 2021; Benish et al., 2020; Zhu et al., 2020; Han et al., 2020; Chen et al., 2023). These vertically observational studies generally indicate that merging of the stable boundary layer, residual layer, and convection-driven mixing layer involves the mixing of trace gases from these different atmospheric layers, and leads to complex vertical O₃ profiles. However, these existing O₃ vertical observations suffer from low observation height (tower-based, tethered-balloon-based, unmanned-aerial-vehicle-based observations), short observation period (tethered-balloon-based, aircraft-based, unmanned-aerial-vehicle-based observations), and low observation accuracy (lidar-based observation), making them less able to provide a complete and accurate O₃ vertical distribution for the whole lower troposphere, not to mention *h*-reference lower-tropospheric O₃ climatology.

To our knowledge, ozonesonde represents the most accurate observation method for O₃ profiles in the troposphere. Therefore, in this study, we collected ozonesonde data observed in Beijing (northern China, Fig. 1a) and Hong Kong (southern China, Fig. 1a) to investigate the *h*-reference O₃ vertical distribution in the lower troposphere over Chinese megacities. In addition, we also considered satellite-based O₃ precursor data, atmospheric composition reanalysis data, an integral method to determine the mixing layer top height *h*, and a photochemical indicator method to diagnose the O₃ production sensitivity. The specific aims of the study were to explore (1) the degree to which lower-tropospheric O₃ over megacities stratifies in the *h*-reference vertical coordinate system; (2) patterns in lower-tropospheric O₃ profiles in the *h*-reference vertical coordinate system; (3) how meteorological and photochemical processes modulate O₃ vertical distribution patterns in the lower troposphere; and (4) differences in the characteristics and mechanisms of lower-tropospheric O₃ vertical distribution between Beijing and Hong Kong. These results of this study offer a reference for better understanding O₃ pollution in urban regions.

2 Data and methods

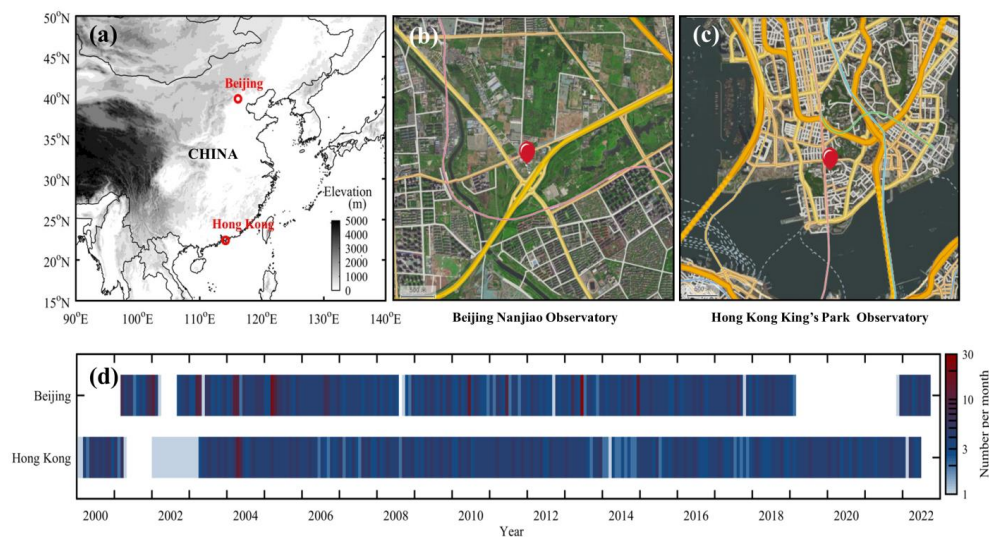


130 **2.1 Ozonesonde measurements**

We used ozonesonde data collected by the Beijing Nanjiao Observatory (116.47°E, 39.80°N, 33 m) and Hong Kong King’s Park Observatory (114.17°E, 22.31°N, 66 m) from 2000 to 2022 (Fig. 1). Beijing Nanjiao Observatory is located in southern suburban of Beijing (Fig. 1b), while Hong Kong King’s Park Observatory is situated within the urban core of Hong Kong (Fig. 1c). Both sites are affected by urban traffic emissions (Fig. 1b and c).

135 Ozonesondes accompanied by radiosondes were regularly launched at approximately 13:30 local standard time (LST) once a week and provided high vertical resolution profiles of O₃, temperature, pressure, and humidity. We excluded data from ozonesondes launched outside a time window of 12:00–15:00 LST in order to minimize changes in mixing layer O₃ arising from different launch times. We interpolated the original profiles on a fixed vertical grid of 20 m vertical resolution. To reduce uncertainties associated with data gaps, we further discarded (i)

140 profiles with > 25% missing data between 0 and 4 km (i.e., accumulated data gaps of > 0.25 × 4,000 = 2,000 m), and/or (ii) profiles with > 10 missing data points between the surface and estimated mixing layer height (i.e., accumulated data gaps of > 10 × 20 = 200 m). After data exclusion, 1,897 ozonesondes were available for study: 924 soundings in Beijing and 973 soundings in Hong Kong. Figure 1d shows the monthly distribution of the available ozonesondes.



145

Figure 1. (a) Coordinates and surrounding environments of ozonesonde sites at (b) Beijing Nanjiao Observatory and (c) Hong Kong King’s Park Observatory. (d) Monthly distribution of the available ozonesonde observations. Map image is © Amap.

150 **2.2 Space-based ozone precursors**

Level-3 formaldehyde (CH₂O, an indicator of VOCs) and nitrogen dioxide (NO₂, an indicator of NO_x) column products from the Ozone Monitoring Instrument (OMI; <https://disc.gsfc.nasa.gov/>) were used to characterize O₃ precursor concentrations and diagnose O₃ production sensitivity. OMI is a nadir-looking near-UV/visible CCD spectrometer aboard the Aura satellite of NASA’s Earth Observing System (Levelt et al., 2018). It provides global observations from 2004 onwards with a transit time at approximately 13:45 LST. Daily Level-3 products covering the period from 2004 to 2022 were adopted. The spatial resolution of the Level-3 CH₂O products is 0.1° × 0.1°, and that of NO₂ is 0.25° × 0.25°; therefore, a bilinear interpolation method was used to resample OMI products to the

155



same resolution ($0.25^\circ \times 0.25^\circ$). We extracted daily data from a 3×3 grid region ($0.75^\circ \times 0.75^\circ$ centered on the ozonesonde site) and then averaged them to represent O_3 precursor columns for the respective sites.

160

2.3 Atmospheric composition reanalysis

Besides the OMI-based column products, pressure-level CH_2O , and NO_2 data from the fourth-generation European Center for Medium-Range Weather Forecasts (ECMWF) Atmospheric Composition Reanalysis (EAC4) were also used to characterize O_3 precursor concentrations and diagnose vertical O_3 production sensitivity. The EAC4 combines model data with global satellite observations into a complete and consistent dataset using a model of the atmosphere based on the laws of physics and chemistry (Inness et al., 2019). It was available at 3-h resolution for a horizontal resolution of $0.75^\circ \times 0.75^\circ$ and a vertical resolution of 7 layers below 700 hPa (1000, 950, 925, 900, 850, 800, and 700 hPa). EAC4 CH_2O and NO_2 data at 06:00 UTC from 2003 onwards were used to support our interpretation of sonde-based O_3 vertical distribution.

170

2.4 Determination of mixing layer top height h

Several approaches have been developed to estimate h based on the gradient variation of individual atmospheric variables from radiosonde data (Seidel et al., 2010), including temperature (T), potential temperature (θ), relative humidity (RH), specific humidity (q), and atmospheric refractivity (N). However, there are substantial differences in the existing methods. Wang and Wang (2014) proposed a three-step method to integrate temperature, humidity, and cloud data to generate a consistent estimate of h from radiosonde profiles: Step 1, identify the height (h_0) that best meets the individual criteria for different atmospheric variables; step 2, derive the location of the cloud; and step 3, determine a consistent mixing layer height (h_{con}). We adopted this integral method to determine the mixing layer heights in Beijing and Hong Kong. Five atmospheric variables, namely, T , θ , RH , q , and N , were used. Among them, T and RH were measured by radiosonde, and the other variables were calculated from T , RH , and atmospheric pressure (Seidel et al., 2010). The upper limit of h was set to 4 km.

175

180

2.5 h -referenced vertical distribution and classification

Once the mixing layer height h was determined, all profiles were expressed in the z/h vertical coordinate system, where z is the actual altitude. In practice, atmospheric variables were interpolated along z/h values ranging between 0 (the surface) and 2 ($2 \times h$) with a vertical resolution of 0.05 (i.e., 41 altitude levels). For instance, if h on a specific profile was 1,000 m, the resampled profile extended from 0 to 2000 m with bins of 50 m. Hereafter, this type of vertical profile is denominated as a mixing-layer-height-referenced (i.e., h -referenced) profile. In this z/h vertical coordinate system, mixing-layer O_3 was denominated as MLO_3 and free-tropospheric O_3 was denominated as FTO_3 . Based on Student's t test, we further classified individual h -referenced O_3 profiles into three distinct patterns: MLO_3 -dominated (mean MLO_3 significantly higher than mean FTO_3 at a significance level of 0.01); FTO_3 -dominated (mean MLO_3 significantly lower than mean FTO_3 at a significance level of 0.01); and uniform distribution (no significant differences between the means of MLO_3 and FTO_3).

190

2.6 Diagnosis of ozone production sensitivity

O_3 is photochemically generated when its precursors (e.g., NO_x and VOCs) are abundant in the presence of sunlight (Seinfeld and Pandis, 2016). Owing to complex chemical mechanisms and regional differences in emissions and meteorology, the relationship between O_3 and its precursors involves highly non-linear interactions (Jin et al., 2020). Under high VOC and low NO_x conditions, O_3 production is not sensitive to VOCs, but is positively correlated to NO_x (i.e., a NO_x -sensitive regime). Under low VOC and high NO_x conditions, O_3 production tends to increase with VOC growth or NO_x reduction (i.e., VOC-sensitive regime). In this study, the

200



CH₂O/NO₂ ratio (FNR) was used as the photochemical indicator to diagnose O₃ production sensitivity. An inherent challenge of this diagnosis approach is that FNR thresholds marking the VOC–NO_x transition regime are likely distinct from region to region (Jin et al., 2020). For the NCP region (including Beijing), Li et al. (2021) diagnosed the transition regime as occurring when FNR ranges from 1.2 to 2.1; for the PRD region (including Hong Kong), Liao et al. (2021) diagnosed the transition regime as occurring when FNR ranges from 1.0 to 1.5. Ratios below and above these ranges indicate VOC-limited O₃ production and NO_x-limited regimes, respectively. These localized FNR thresholds were adopted in this study to diagnose O₃ production sensitivity.

210 3 Results and discussion

3.1 Lower-tropospheric ozone climatology

Figure 2 shows the traditional lower tropospheric O₃ climatology of Beijing and Hong Kong. Seasonal results are averaged from ozonesonde profiles collected in spring (M–A–M), summer (J–J–A), autumn (S–O–N), and winter (D–J–F). There is a typical summer-high-winter-low seasonality in lower tropospheric O₃ over Beijing, with the highest O₃ concentrations in June. Such seasonality is broadly similar to previous tropospheric O₃ climatology based on lesser O₃ profiles in Beijing (Ding et al., 2008; Zhang et al., 2021). In photochemical active months (May–August), high-concentration O₃ is photochemically produced throughout the lower troposphere, particularly in the mixing layer, causing an isolated O₃-peak area (> 100 ppbv) near the upper mixing layer. In other months, strong urban NO-titration accompanied by weak O₃ production causes a positive vertical gradient of O₃ concentration in the lower troposphere; the average vertical gradient of O₃ reaches a maximum in winter.

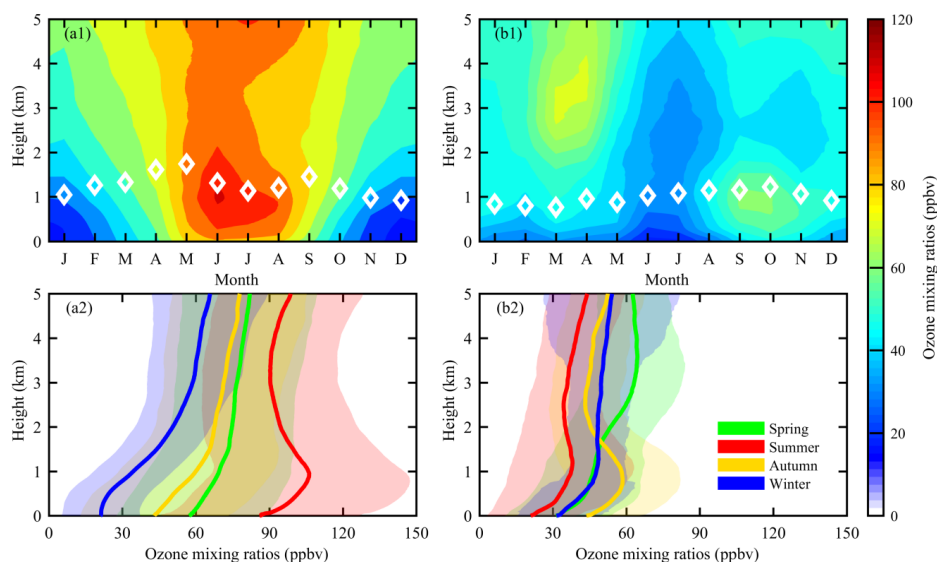


Figure 2. Lower tropospheric ozone vertical distribution over (a) Beijing and (b) Hong Kong. (1) Monthly variation. (2) Seasonal variation. The white diamonds in (1) represent the monthly mean mixing layer height.

225 Lower tropospheric O₃ climatology in Hong Kong is remarkably different from that in Beijing. In particular, lower tropospheric O₃ is low in the summertime (< 40 ppbv). Similar O₃ minima have been reported in other subtropical cities in Eastern Asia, such as Hanoi and Naha (Liao et al., 2021; Oltmans et al., 2004; Ogino et al., 2013) and likely reflect the influence of the Asian summer monsoons, which bring maritime air with low O₃ northward



230 from the tropical Pacific to subtropical regions. Although Beijing is also impacted by the Asian summer monsoons,
 these ocean-sourced air masses become enriched with O₃ precursors while passing over polluted eastern China,
 leading to an accumulation of O₃ over Beijing. Interestingly, there are two isolated areas of O₃ enhancement over
 Hong Kong, those in the lower free troposphere (~3.5 km) from March to April and in the upper mixing layer (~0.8
 km) in autumn. The former is attributed to long-range transport of wildfire-related O₃ production in the upwind
 Indochina Peninsula; the latter results from local O₃ production via photochemical reactions under hot and dry
 235 weather conditions in autumn (Liao et al., 2021).

3.2 Mixing-layer-height-referenced ozone vertical distribution

We investigated the climatological vertical stratification of O₃ below and above the ML–FT interface (i.e.,
 mixing layer height h) over Beijing and Hong Kong (Fig. 3). This h -referenced O₃ climatology provides an
 240 additional dimension (further categorization by mixing layer height) not available in traditional vertical ozone
 profile climatology. The significant disparity between the h -referenced O₃ climatology (Fig. 3) and traditional O₃
 climatology (Fig. 2) illustrates how much information is lost using simple ozonesonde averages. For example, the
 h -referenced O₃ profiles show a clear inflexion (or discontinuity) at the interface between the ML and FT ($z/h=1$),
 which is not apparent in the traditional O₃ climatology. These results reflect the fact that mixing-layer capping
 245 inversion acts as an effective although porous geophysical barrier that limits vertical exchange between the ML and
 FT, leading to distinct O₃ levels on either side.

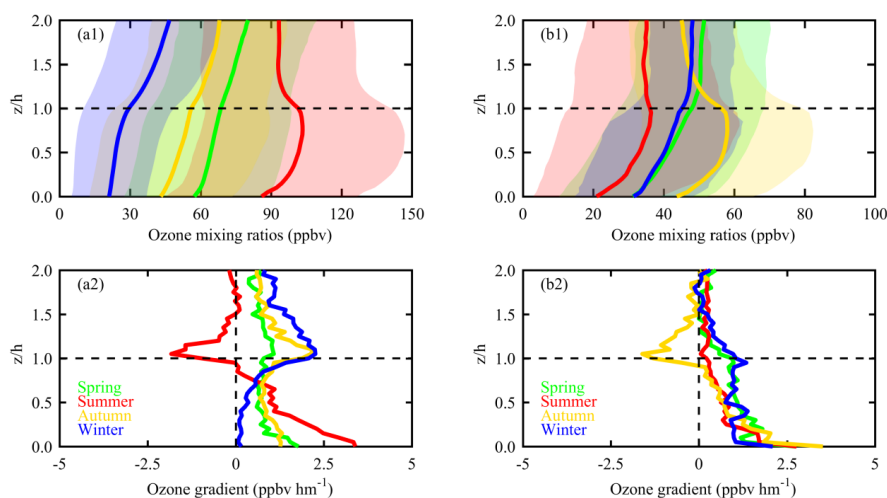


Figure 3. Mixing-layer-height-referenced ozone vertical distribution over (a) Beijing and (b) Hong Kong. (1) Ozone
 250 mixing ratio profile. (2) Ozone gradient profile.

250

In Beijing, seasonal O₃ profiles in autumn, winter, and spring present a low-ML/high-FT vertical distribution
 pattern with O₃ mixing ratios that increase with altitude throughout the lower troposphere and variable vertical
 gradients depending on season and altitude. Generally, the strongest gradients are observed either close to the
 surface or near the ML–FT interface. Near the surface, they are likely due to strong O₃ titration by NO emitted from
 255 urban traffic (Karl et al., 2023). Near the ML–FT interface, they are likely attributable to the barrier effect of
 mixing-layer capping inversion. The O₃ gradients gradually decrease with altitude above the ML–FT interface;
 below the interface, they slightly decrease with altitude in spring and autumn but gradually increase with altitude in



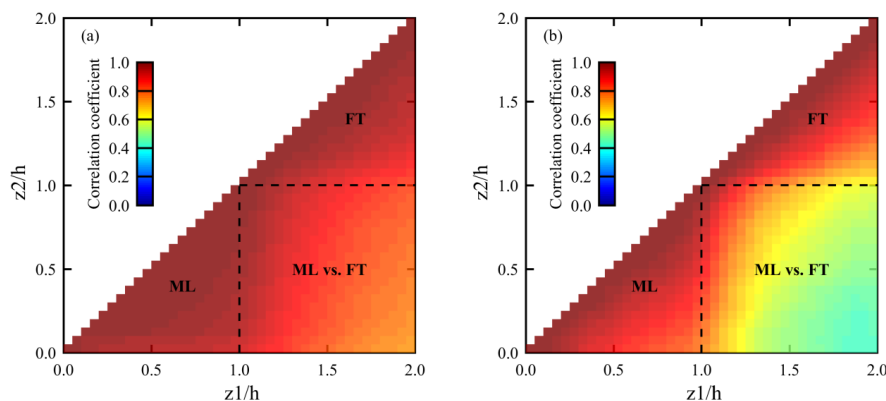
winter. Winter O_3 gradients are almost zero in the surface layer ($z/h < 0.4$), reflecting strong titration that often causes O_3 to be almost completely depleted in the lower ML. In summer, the averaged O_3 profile exhibits a sickle-shape pattern, with a marked drop in concentrations from the upper ML to the lower FT. Summer O_3 gradients quickly decrease with altitude inside the ML and eventually become negative near the ML–FT interface. The maximum negative gradient (-2.2 ppbv hm^{-1}) occurs just above the mixing layer top height. In Hong Kong, the averaged O_3 profiles in winter and spring present low-ML/high-FT vertical distribution, similar to Beijing. However, the autumn averaged O_3 profile shows a sickle-shape pattern, similar to the summer profile in Beijing. In contrast, the summer averaged O_3 profile in Hong Kong displays a transitional feature from spring to autumn, characterized by a weak O_3 peak just below the ML–FT interface. Compared with Beijing, the O_3 gradients in Hong Kong vary across a smaller range; however, they are commonly sharper in the surface layer.

For both Beijing and Hong Kong, the highly variable O_3 gradients in the ML confirm that the well-mixed ML remains a large exception for O_3 , even on summer afternoons when vertical turbulent mixing is expected to be strongest. In particular, the increasing O_3 with altitude in the lower ML indicates that strong photochemistry and vertical mixing on summer afternoons is insufficient to quickly compensate for O_3 titration consumption ($NO+O_3 \rightarrow NO_2$) in the surface layer, where NO is largely emitted by urban traffic. A previous study indicated that MLO_3 evolution in urban areas adheres to vertical physiochemical circulation involving multiple reactions in the O_3 –NO– NO_2 triad (Tang et al., 2017). NO emissions react with O_3 to generate NO_2 near the ground, which is then transported vertically to the upper ML; O_3 is generated by NO_2 photolysis in the upper ML and is then transported down to the surface layer to compensate for the loss by NO titration. In this process, the titration process is thought to drive the downward flux of O_3 into the urban roughness layer (Karl et al., 2023). Under favorable weather conditions, high-concentration MLO_3 production can greatly modify the vertical profile of O_3 from the more customary low-ML/high-FT vertical distribution to a high-ML/low-FT vertical distribution. This modification is thought to be episodic in low-emission cities (e.g., Frankfurt; (Petetin et al., 2016); in such cities, the vertical structure of averaged O_3 profiles in the photochemical active season (e.g., summer) remains low-ML/high-FT the same throughout the year (Petetin et al., 2018). However, in high-emission megacities (e.g., Beijing and Hong Kong), photochemistry-driven modification can be expected to be common during in the photochemical active season (summer in Beijing and autumn in Hong Kong), eventually causing a seasonal sickle-shape O_3 profile in the lower troposphere. These seasonal differences in lower tropospheric O_3 profiles imply that the aforementioned transport barrier to vertical exchange has different connotations, typically changing from a ML-to-FT detrainment barrier in summer (autumn) to a FT-to-ML entrainment barrier in other seasons in Beijing (Hong Kong).

The vertical autocorrelation of O_3 in the z/h vertical coordinate system was further analyzed to investigate the links between the ML and FT. Based on all individual O_3 profiles, we calculated the correlation coefficients of O_3 between the different pairs of z/h altitude levels. The obtained O_3 vertical autocorrelation matrix is shown in Figure 4. Within both the ML (z/h between 0 and 1) and FT (z/h between 1 and 2), we found strong correlations (usually > 0.90 , mean of 0.97 in Beijing; > 0.85 , mean of 0.91 in Hong Kong). However, the correlations between the two atmospheric compartments (ML vs. FT) decreased quickly with vertical distance, with means of 0.84 in Beijing and 0.60 in Hong Kong. In general, correlations in Hong Kong were found to be weaker than those in Beijing. This can be explained by two possible reasons. (i) Hong Kong is a coastal city, where clean maritime air and polluted continental air can dominate at different altitudes (e.g., sea-land breeze); therefore, distinct air mass sources can weaken the correlation of O_3 between different altitude levels. (ii) Hong Kong is located in humid zone, where surface sensible heat is relatively weaker than that in semi-humid zones (e.g., Beijing); therefore, weak turbulent convection causes weak mixing of O_3 in the vertical direction (Xu et al., 2021). The iso-correlation contours in both



megacities present a “W” shape along the diagonal direction, with the inflexion point at $z/h = 1$. This is consistent with northern mid-latitude findings in Petetin et al. (2018), indicating that stratification occurs most commonly at the ML–FT interface.



305

Figure 4. Auto-correlation of ozone mixing ratios between different z/h altitude levels over (a) Beijing and (b) Hong Kong. Dashed lines separate three areas involving correlation within the mixing layer (ML), within the free troposphere (FT), and between the mixing layer and free troposphere (ML vs. FT).

310 Both surface concentration and vertical distribution of O_3 are highly variable at the synoptic scale and can greatly depart from standard climatology depending on meteorological conditions and the availability of O_3 precursors. Based on Student's t test, all individual h -referenced O_3 profiles were further classified into three typical patterns to investigate synoptic climatology of lower tropospheric O_3 in Beijing and Hong Kong. The statistical results indicate that the FTO_3 -dominated pattern occurs most frequently in both megacities. The respective occurrence frequencies of FTO_3 -dominated, uniform, and MLO_3 -dominated distributions were 69%, 11%, and 20%
 315 in Beijing, and 54%, 21%, and 25% in Hong Kong, respectively. Figure 5 shows the composite of O_3 (gradient) profiles according to the different O_3 profile patterns in Beijing and Hong Kong. In the FTO_3 -dominated pattern, averaged FTO_3 concentrations are 61.6 ppbv in Beijing and 44.9 ppbv in Hong Kong, which are 15 and 13 ppbv higher than the averaged MLO_3 concentrations in the respective cities. Such concentration differences between FTO_3 and MLO_3 cause a sharp positive gradient of O_3 near the ML–FT interface (2.3 ppbv hm^{-1} in Beijing and 1.8 ppbv hm^{-1} in Hong Kong). For the MLO_3 -dominated pattern, averaged MLO_3 concentrations are 109.8 ppbv in Beijing and 62.2 ppbv in Hong Kong, ~18 ppbv higher than the averaged FTO_3 concentrations in both cities, causing a steep negative gradient of O_3 near the ML–FT interface (−4.3 ppbv hm^{-1} in Beijing and −3.8 ppbv hm^{-1} in Hong Kong). For the uniform distribution, despite no significant difference in the means of MLO_3 and FTO_3 , the composited O_3 profile shows an “S” shape pattern with a slightly negative gradient (approximately −1.0 ppbv hm^{-1})
 320 near the ML–FT interface.
 325

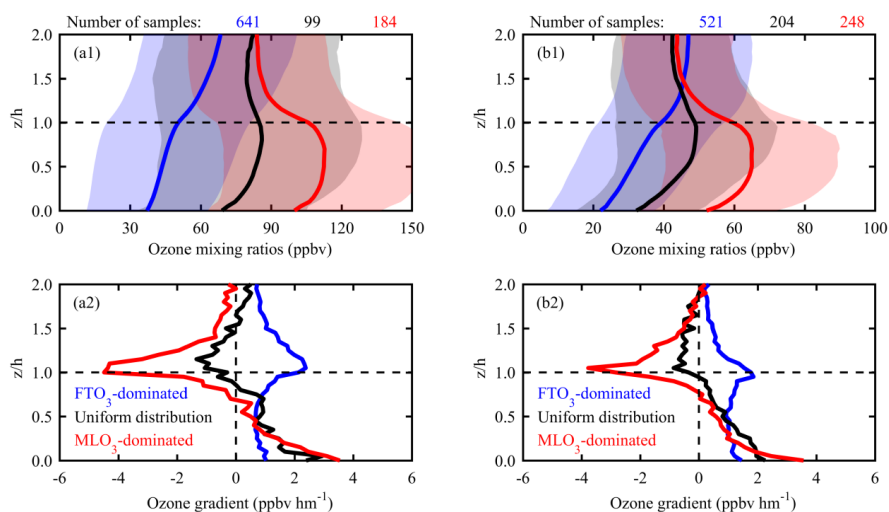


Figure 5. Composites of (1) h -referenced ozone profiles and (2) h -referenced ozone gradient profiles according to different patterns in (a) Beijing and (b) Hong Kong.

Figure 6 shows occurrence frequencies of the three distinct O_3 profile patterns in different seasons and mixing layer height bins. In Beijing, while the FTO_3 -dominated pattern prevails in winter (94.2%), autumn (79.1%), and spring (75.3%), the MLO_3 -dominated pattern prevails in summer (46.3%). In Hong Kong, the FTO_3 -dominated pattern occurs frequently in spring (67.7%), winter (65.8%), and summer (55.8%), and the MLO_3 -dominated pattern prevails in autumn (55.1%). Such frequent occurrence of MLO_3 -dominated patterns confirms our theory that the MLO_3 -dominated pattern is common rather than episodic in the photochemical active season of high-emission Chinese megacities. In contrast, the occurrence dependence of O_3 profile patterns on mixing layer height is not as strong as that on season. The FTO_3 -dominated pattern prevails in most h bins, particularly in Beijing. Nevertheless, the MLO_3 -dominated pattern is still relatively more frequent in the h bin between 1.0 and 2.0 km (27.3% in Beijing and 36.7% in Hong Kong) than in lower and higher h bins. This is to some degree consistent with the findings of Zhao et al. (2019), who revealed that moderate mixing layer height is usually accompanied by very favorable meteorological (moderate RH and high temperature) and photochemical (NO_x -VOC transition regime) conditions for high-concentration MLO_3 production.

345

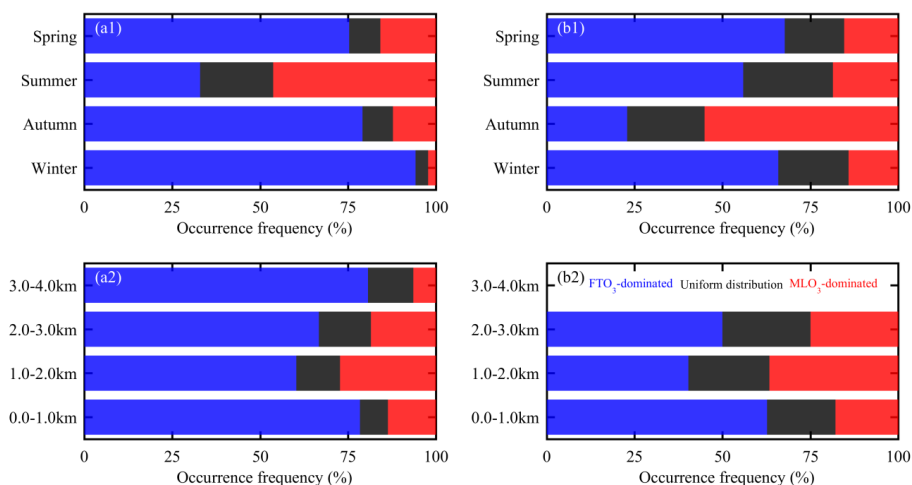


Figure 6. Occurrence frequencies of three h -referenced ozone profile patterns according to (1) season and (2) mixing layer height bins in (a) Beijing and (b) Hong Kong (in Hong Kong, no case is found for $h > 3.0$ km).

3.3 Mechanistic understanding of distinct ozone profile patterns

3.3.1 Meteorological interpretations

The h -referenced profiles of potential temperature (θ), relative humidity (RH), and wind speed (WS) according to different O_3 profile patterns in Beijing and Hong Kong are shown in Figure 7. Near the surface ($z/h < 0.1$), potential temperature decreases with altitude in both megacities, indicating a shallow superadiabatic layer due to daytime surface radiation heating. As expected, in other parts of the ML, potential temperature profiles in Beijing are neutral adiabatic within the afternoon convective ML (Stull, 1988). However, the corresponding profiles in Hong Kong are subadiabatic, implying insufficient thermal convection mixing over this coastal city, which may partly explain the lower autocorrelations of O_3 between different altitude levels within the ML in Hong Kong (Fig. 4). In the FT ($z/h > 1.0$), potential temperature increases with altitude with a relatively larger gradient than that in the ML. As expected, there is a sharp increase in potential temperature at the ML–FT interface where positive vertical gradients reach $1.0 \text{ }^\circ\text{C hm}^{-1}$ on average. This maximum gradient is indicative of strong mixing layer capping inversion. However, the maximum gradient values are almost identical among the different O_3 profile patterns, suggesting that capping inversion acts as a transport barrier to suppress O_3 vertical exchange but is not responsible for the different directions of vertical exchange (i.e., FT-to-ML entrainment or ML-to-FT detrainment). In fact, no structural change was found in the averaged θ profiles among the different patterns. Similar to the θ profiles, the RH and WS profiles shared an analogous vertical structure among different O_3 profile patterns in both megacities. In general, RH and WS levels inside the ML were higher and lower, respectively, than the corresponding lower troposphere levels.

Without considering the vertical structure, values of aforementioned meteorological variables differed among the O_3 profile patterns, suggesting that meteorological conditions are the main regulating factors of lower troposphere O_3 levels. From the FTO_3 -dominated to MLO_3 -dominated pattern, potential temperature increases in both megacities. The high temperature of the MLO_3 -dominated pattern favors high-concentration O_3 production in the ML. The cross-pattern value change of RH and WS shows some differences between Beijing and Hong Kong. For example, on MLO_3 -dominated days, RH is moderate in Beijing but low in Hong Kong, and when WS is low in Beijing it is moderate in Hong Kong. Nevertheless, RH and WS inside the ML of Hong Kong are always higher



than those in the ML of Beijing. While humid air tends to suppress photochemical reactions, windy condition tends to inhibit ozone accumulation. The higher RH and WS conditions may partly explain the lower O₃ levels in Hong Kong. From above analyses a key factor leading to the MLO₃-dominated pattern in both megacities is high temperature. Previous studies have indicated that high temperature not only increases the O₃ production rate (Wang et al., 2022a), but also strengthens the volatilization rate of O₃ precursors, particularly biomass VOC emissions (Duncan et al., 2009).

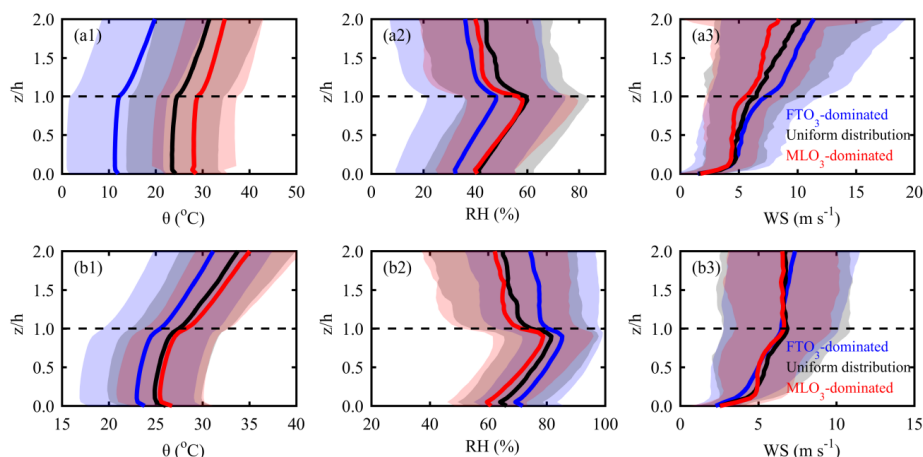


Figure 7. Composited *h*-referenced profiles of (1) potential temperature, (2) relative humidity, and (3) wind speed according to different ozone profile patterns in (a) Beijing and (b) Hong Kong.

385

3.3.2 Photochemical interpretations

Figure 8 shows composited column concentrations and vertical distributions of CH₂O and NO₂ according to the different O₃ profile patterns. In Beijing, tropospheric CH₂O columns are $7.7 (\pm 4.3) \times 10^{15}$, $11.8 (\pm 6.9) \times 10^{15}$, and $12.4 (\pm 5.7) \times 10^{15}$ molec. cm⁻² in the FTO₃-dominated, uniform distribution, and MLO₃-dominated patterns, respectively; the corresponding values for the tropospheric NO₂ column are $19.2 (\pm 10.7) \times 10^{15}$, $14.5 (\pm 9.8) \times 10^{15}$, and $13.2 (\pm 7.7) \times 10^{15}$ molec. cm⁻², respectively. From the FTO₃-dominated pattern to the MLO₃-dominated pattern, CH₂O increases throughout the lower troposphere (up to 700 hPa) with a maximum increment in the upper ML (~900 hPa). This maximum increment can be explained by high-elevation biogenic VOC emissions in the western mountains (i.e., Taihang Mountains) and vertical mixing of VOC emissions in the southern NCP during the transport process. In contrast, NO₂ mainly decreases in the lower ML (below 900 hPa), especially in the surface layer (1000 hPa). The cross-pattern change of O₃ precursors is likely attributable to significant seasonality of precursor emissions in Beijing and the NCP (e.g., anthropogenic emissions change between heating and non-heating periods and natural emissions change between leafy and leafless periods). As shown in Figure 6, the MLO₃-dominated pattern prevails in the warm season (Spring–Autumn), during which heating-related precursor emissions (mainly NO_x) are negligible but biogenic precursor emissions (mainly VOCs) are considerable (Fig. 7). This explains the elevated CH₂O column and low NO₂ column in the MLO₃-dominated pattern in Beijing.

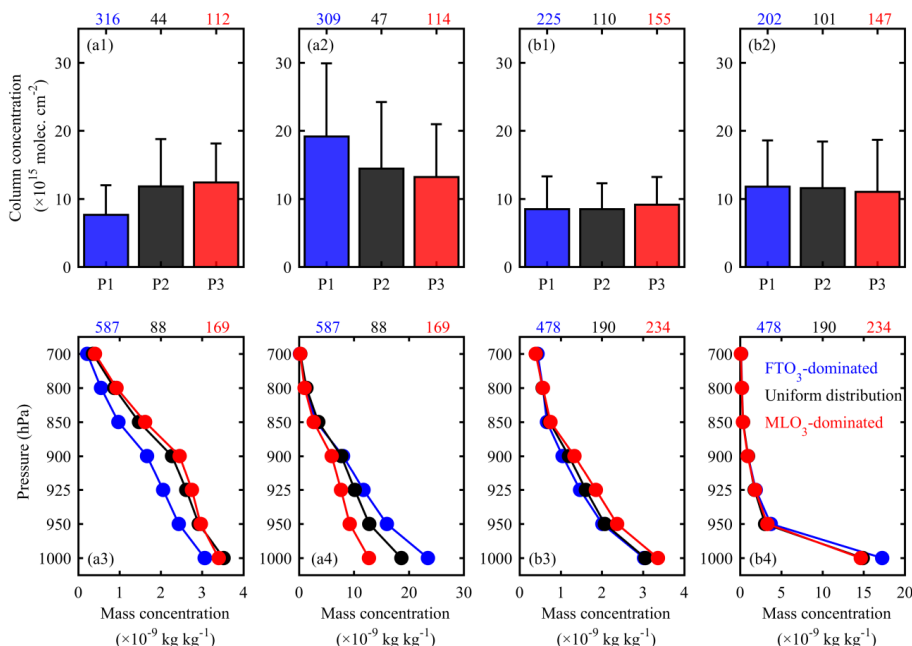
395

In Hong Kong, both CH₂O and NO₂ had lower concentrations than those in Beijing (except for CH₂O in the FTO₃-dominated pattern). This partly explains the lower O₃ levels in Hong Kong. The cross-pattern change of O₃ precursors (regardless of total column or vertical distribution) in Hong Kong follows the same order as that in Beijing (i.e., increase of CH₂O and decrease of NO₂ from FTO₃-dominated to MLO₃-dominated). In Hong Kong,

405



410 tropospheric CH₂O columns are $8.5 (\pm 4.8) \times 10^{15}$, $8.5 (\pm 3.8) \times 10^{15}$, and $9.1 (\pm 4.1) \times 10^{15}$ molec. cm⁻² in the FTO₃-dominated, uniform distribution, and MLO₃-dominated patterns, respectively. The corresponding values for tropospheric NO₂ columns are $11.8 (\pm 6.8) \times 10^{15}$, $11.6 (\pm 6.8) \times 10^{15}$, and $11.0 (\pm 7.6) \times 10^{15}$ molec. cm⁻². Evidently, cross-pattern change amplitudes of O₃ precursors in Hong Kong are smaller than those in Beijing. In subtropical Hong Kong and the PRD region, O₃ precursor emissions are not affected by heating-related emission changes from warm to cold season, and are less affected by seasonal biogenic emission changes because of evergreen leaves throughout the year. This weak seasonal dependence of precursor emission leads to small cross-pattern differences in CH₂O and NO₂ in Hong Kong. The slight differences in O₃ precursors among the different O₃ profile patterns in Hong Kong are likely attributable to temperature-driven precursor changes. Higher temperatures in the MLO₃-dominated regime trigger the release of VOC emissions, causing higher CH₂O concentrations, and photolysis of NO₂, causing lower NO₂ concentrations.



420 Figure 8. Composite column concentrations (upper panel) and vertical distributions (lower panel) of ozone precursors according to different ozone profile patterns in (a) Beijing and (b) Hong Kong. CH₂O (1 and 3); NO₂ (2 and 4). P1: FTO₃-dominated pattern; P2: Uniform distribution pattern; P3: MLO₃-dominated pattern.

425 O₃ production chemistry in urban areas is usually VOC-limited (Li et al., 2021), and we found that CH₂O concentrations in both Beijing and Hong Kong increased from the FTO₃-dominated to the MLO₃-dominated pattern, suggesting increased potentiality of high-concentration O₃ production. This potentiality can be easily realized on the MLO₃-dominated days owing to the hot-dry weather conditions, providing favorable meteorology for photochemical reactions. That is to say, the MLO₃-dominated pattern in Beijing and Hong Kong is driven by intensive photochemical production of MLO₃ under elevated VOC and high temperature conditions. Since the increment of CH₂O is larger in the upper mixing layer, higher-concentration O₃ production can be expected in upper mixing layer, in consistent with the observational result of sickle-shape O₃ profile in the lower troposphere. Conversely, the FTO₃-dominated pattern is likely due to strong titration consumption of MLO₃ under elevated NO₂



and low temperature conditions. Owing to the nonlinear relationship between O_3 and its precursors (i.e., VOC and NO_x), net production of O_3 is subject to both absolute concentrations of VOC and NO_x and their relative ratio, which determines the O_3 production sensitivity. Based on the FNR photochemical indicator method, we further
435 diagnosed O_3 production sensitivity to examine the potential change in O_3 production chemistry among different O_3 profile patterns.

Figure 9 shows the scatter distribution of OMI-based tropospheric CH_2O and NO_2 columns over Beijing and Hong Kong. In Beijing, most (~90%) points associated with the FTO_3 -dominated pattern are located in the
440 VOC-limited regime; these points correspond to high NO_2 concentrations, indicating large O_3 consumption via the titration reaction ($NO+O_3\rightarrow NO_2$). Strong titration can therefore partly explain the low MLO_3 concentrations in the FTO_3 -dominated pattern (another explanation is weak O_3 production due to low temperature). In other patterns, ~27% of days are identified as being in the transition regime, which usually represents optimal VOC- NO_x ratios for net production of O_3 . High-efficiency O_3 production likely offsets NO -titration O_3 consumption, leading to higher
445 MLO_3 concentration compared with that in the FTO_3 -dominated pattern. In contrast, in Hong Kong, points that belong to different O_3 profile patterns mix well together, forming similar frequency matrices of O_3 production sensitivity among the different patterns. Compared with the rare occurrence of the NO_x -limited regime in Beijing, the NO_x -limited regime is more common in Hong Kong (> 20%), indicating that ozone production chemistry is more sensitive to NO_x in Hong Kong than in Beijing. Since the partly integral concentration of O_3 precursors in the
450 lower layer holds a significantly higher proportion of the total column concentration, the OMI-based analyses are more likely to represent near-surface characteristics of O_3 production sensitivity, particularly in Hong Kong (Fig. 8). Therefore, it is necessary to further explore the vertical characteristics of O_3 production sensitivity.

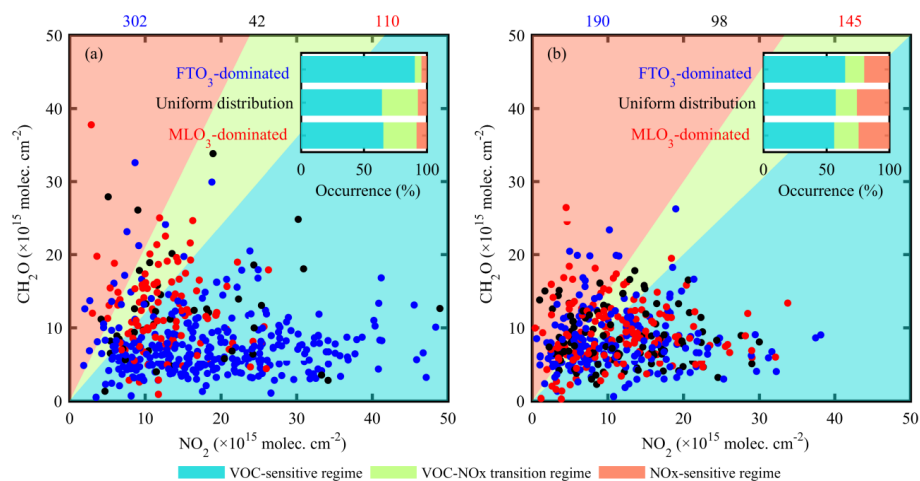
Figure 10 shows the EAC4-based vertical characteristics of O_3 production sensitivity. In Beijing, the averaged
455 FNR values in the ML (< 850 hPa) differ significantly among the different O_3 profile patterns. However, all are located in the VOC-limited regime. From 850 to 700 hPa, the averaged FNR values increase quickly, causing a shift of O_3 production sensitivity from VOC-limited to NO_x -limited. There is a significant increase of the transition from FTO_3 -dominated to MLO_3 -dominated, whereas the occurrence of the VOC-limited regime shows an opposite trend. Vertically, the transition regime frequency increases with height in the ML (< 850 hPa), regardless of the O_3 profile
460 pattern. This is broadly similar to the MAX-DOAS-based findings of Chi et al. (2018), who reported that the transition regime accounted for 27.3% at 300 m height, but 50.0% at 1,100 m height over Beijing. In Hong Kong, FNR values increase more rapidly with height than in Beijing, but show small differences among the different O_3 profile patterns. The shift height of O_3 production sensitivity in Hong Kong is lower than that in Beijing. Based on averaged FNR profiles, the shift in Hong Kong occurs in the height range between 950 and 925 hPa. The daily
465 occurrence statistics also reveal a higher transition regime frequency in this height range. Below this height, O_3 production chemistry is overwhelmingly controlled by the VOC-limited regime, and above by the NO_x -limited regime. Similar results had been reported via MAX-DOAS observations in Guangzhou (a megacity ~110 km northwest of Hong Kong), where O_3 production sensitivity changed with height from VOC-limited (0.02–0.22 km) to transitional (0.22–0.42 km) to NO_x -limited (0.42–2.02 km) (Lin et al., 2022).

470 The above results demonstrate that the ozone precursor level and ozone production sensitivity play an important role in modulating the vertical distribution of O_3 in the lower troposphere. To be specific, the changes of ozone precursor level and ozone production sensitivity determine the final chemical behavior of O_3 (destruction or production) in the mixing layer among the different O_3 profile patterns. In the FTO_3 -dominated pattern, the
475 supersaturated NO_x concentrations trigger significant MLO_3 destruction under the overwhelming VOC-limited



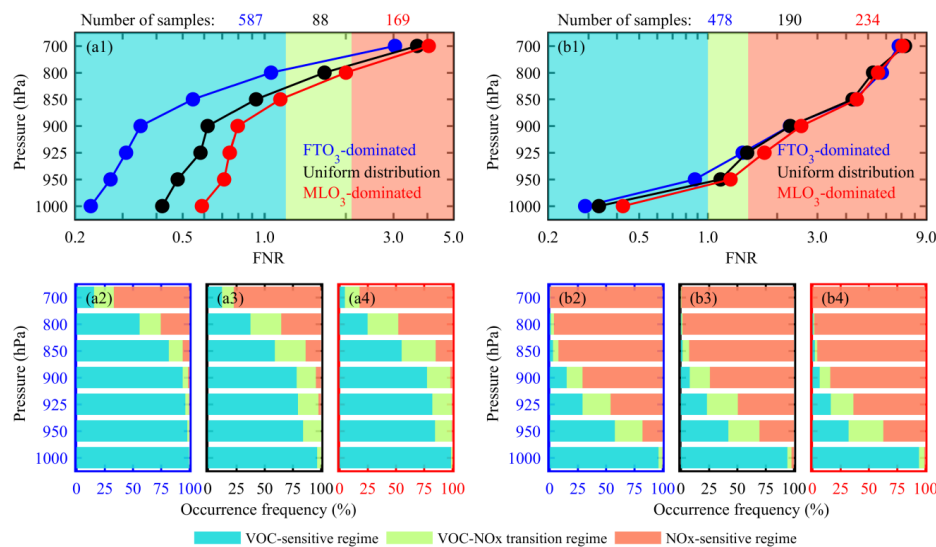
regime condition, causing a significantly lower O_3 in the mixing layer than that in the free troposphere. Therefore, the mixing layer capping inversion acts as a barrier for FT-to-ML O_3 entrainment in the FTO_3 -dominated pattern. From the FTO_3 -dominated pattern to MLO_3 -dominated pattern, the increased CH_2O concentrations push O_3 production sensitivity away from the VOC-limited regime (towards higher NO_x sensitivity) and favor for ozone photochemically production. The net production of O_3 is expected to be larger in the upper mixing layer, where larger increase of CH_2O occurs. As a result, the MLO_3 -dominated pattern is expressed as a sickle-shape O_3 profile (the highest O_3 level in the upper mixing layer), reflecting a ML-to-FT O_3 detrainment barrier effect of mixing layer capping inversion.

480



485

Figure 9. Ozone production sensitivity of different ozone profile patterns in (a) Beijing and (b) Hong Kong. Scatter distribution of CH_2O and NO_2 in different ozone production sensitivity regimes (1 and 3); statistical occurrence of daily ozone production sensitivity (2 and 4).



490



Figure 10. Vertical characteristics of ozone production sensitivity according to different ozone profile patterns in (a) Beijing and (b) Hong Kong. Upper panels (1) denote vertical FNR profiles. Lower panels (2, 3, and 4) denote the occurrence frequency of ozone production sensitivity in FTO₃-dominated, uniform distribution, and MLO₃-dominated patterns.

495

4 Summary

We investigate lower tropospheric O₃ distribution over two Chinese megacities (Beijing and Hong Kong) by introducing a novel mixing-layer-height-referenced (*h*-referenced) O₃ climatology, in which lower tropospheric O₃ profiles are scaled according to the mixing layer top heights. Mixing layer top height was determined by an integral method that integrates temperature, humidity, and cloud profiles. We focused on the lower troposphere (below 2× the mixing layer top height), with each profile subdivided in two compartments: the mixing layer and free troposphere (ML and FT). By examining O₃ concentration differences between the ML and FT (i.e., MLO₃ and FTO₃), all individual O₃ profiles were classified into three typical patterns: MLO₃-dominated, FTO₃-dominated, and uniform distribution. Sonde-based meteorological profiles and multi-source O₃ precursors (CH₂O and NO₂) were further analyzed to characterize the main physiochemical processes driving contrasting O₃ budgets among the different O₃ profile patterns. Our conclusions are as follows:

510

(1) Compared with traditional sea-level-referenced climatology, *h*-referenced O₃ climatology preserves the dependence of O₃ abundance and its variability on mixing layer top height, highlighting an inflexion point (or discontinuity) at the interface between the ML and FT.

515

(2) Lower tropospheric O₃ concentrations show summer-high/winter-low climatology in Beijing, and autumn-high/summer-low climatology in Hong Kong. In the photochemical active season (summer in Beijing and autumn in Hong Kong), seasonal O₃ profiles exhibit a sickle-shape pattern with a marked drop in concentrations from high values in the upper ML to low values in the lower FT. This sickle-shape profile pattern is significantly different from monotone increasing profile patterns across the rest of the year.

520

(3) Highly variable O₃ gradients in the lower troposphere, particularly at the surface layer and ML–FT interface, reflect the universality of vertical O₃ stratification structure. O₃ stratification in Hong Kong is stronger than that in Beijing. The stratification in the surface layer is likely due to strong titration chemical processes, and that at the ML–FT interface is attributable to the dynamic transport barrier of mixing layer capping inversion on vertical exchange. The contrasting O₃ gradients at the ML–FT interface indicate different transport barrier effects, which typically shift from a ML-to-FT detrainment barrier in summer (autumn) to a FT-to-ML entrainment barrier in other seasons in Beijing (Hong Kong).

525

(4) FTO₃-dominated pattern represents the most common O₃ profile patterns in both Beijing and Hong Kong (occurrence frequencies of 69% and 54%, respectively). However, MLO₃-dominated pattern prevails in the photochemical active season, accounting for 46% of summer days in Beijing and 55% of autumn days in Hong Kong, which is more frequent than the previously reported episodic occurrence in northern mid-altitudes, indicating intensive MLO₃ production in high-emission Chinese megacities.

530

(5) There are no structural differences in lower tropospheric meteorological profiles (θ , RH, and WS) among the different O₃ profile patterns. The maximum positive θ gradient at the ML–FT interface demonstrates the common existence of mixing layer capping inversion, which acts as a barrier to vertical exchange. In the FTO₃-dominated pattern, MLO₃ chemistry is dominated by strong titration consumption under low temperature and high-NO₂ conditions. Therefore, mixing layer capping inversion acts as a barrier in FT-to-ML entrainment. In the MLO₃-dominated pattern, MLO₃ chemistry is dominated by strong photochemical production under high temperature and high-CH₂O conditions. Therefore, mixing layer



535 capping inversion acts as a barrier in ML-to-FT detrainment.
(6) From the FTO₃-dominated to MLO₃-dominated pattern, the O₃ precursor CH₂O (NO₂) substantially
increases (decrease) in Beijing, but increases (decreases) slightly in Hong Kong. Over both megacities, the
CH₂O increment is larger in the upper ML, whereas the NO₂ decrement is larger in the lower ML. Such
540 changes in O₃ precursors push O₃ production sensitivity away from the VOC-limited regime (towards higher
NO_x sensitivity) and facilitate net production of O₃ via photochemical reactions, particularly in the upper
ML.

Comparing the above results with previous northern mid-latitude observations (Petetin et al., 2018), lower
troposphere O₃ variability over high-emission Chinese megacities is more likely controlled by O₃-related chemical
545 processes, including titration consumption and photochemical production. From our comparison of Beijing and
Hong Kong, lower troposphere O₃ variability in China is not only subject to precursor emissions, but also reflects
local topographical and meteorological characteristics. Therefore, to achieve comprehensive understanding of lower
troposphere O₃ variability in China, more ozonesonde observations over more sites are needed in the future.

550 **Data availability**

Ozonesonde data for Beijing are available from the first author upon reasonable request (lzhiheng118@163.com).

Ozonesonde data for Hong Kong are available at <https://woudc.org/home.php?lang=en>.

OMI-based ozone precursor data are available at <https://disc.gsfc.nasa.gov/>.

EAC4-based ozone precursor reanalysis data are available at <https://ads.atmosphere.copernicus.eu/>.

555

Author contributions

ZL and SF designed the research. ZL organized and wrote the manuscript. MG and JQ edited the manuscript. JS
contributed to satellite data analysis and code writing. JZ and YP contributed to ozonesonde observations in Beijing.
All authors contributed to the revision of the manuscript.

560

Competing interests

The contact author has declared that none of the authors has any competing interests.

Disclaimer

565 Publisher's note: Copernicus Publications remains neutral with regard to jurisdictional claims in published maps
and institutional affiliations.

Financial support

This work is supported by the major project of Basic and Applied Basic Research project of Guangdong Province
570 (grant no. 2020B0301030004), the Key-Area Research and Development Program of Guangdong Province (grant
no. 2020B1111360003), the National Natural Science Foundation of China (grant no. 42293321 and 41975181).

References

575 Benish, S. E., He, H., Ren, X. R., Roberts, S. J., Salawitch, R. J., Li, Z. Q., Wang, F., Wang, Y. Y., Zhang, F., Shao, M., Lu, S. H.,
and Dickerson, R. R.: Measurement report: Aircraft observations of ozone, nitrogen oxides, and volatile organic
compounds over Hebei Province, China, *Atmos Chem Phys*, 20, 14523-14545, 10.5194/acp-20-14523-2020, 2020.
Berkes, F., Hoor, P., Bozem, H., Kunkel, D., Sprenger, M., and Henne, S.: Airborne observation of mixing across the
entrainment zone during PARADE 2011, *Atmos. Chem. Phys.*, 16, 6011-6025, 10.5194/acp-16-6011-2016, 2016.



- Chen, Z., Xie, Y., Liu, J., Shen, L., Cheng, X., Han, H., Yang, M., Shen, Y., Zhao, T., and Hu, J.: Distinct seasonality in vertical variations of tropospheric ozone over coastal regions of southern China, *Sci Total Environ*, 874, 162423, <https://doi.org/10.1016/j.scitotenv.2023.162423>, 2023.
- Chi, X. Y., Liu, C., Xie, Z. Q., Fan, G. Q., Wang, Y., He, P. Z., Fan, S. D., Hong, Q. Q., Wang, Z., Yu, X. W., Yue, F. E., Duan, J. B., Zhang, P. F., and Liu, J. G.: Observations of ozone vertical profiles and corresponding precursors in the low troposphere in Beijing, China, *Atmos Res*, 213, 224-235, [10.1016/j.atmosres.2018.06.012](https://doi.org/10.1016/j.atmosres.2018.06.012), 2018.
- 585 Diab, R. D., Thompson, A. M., Mari, K., Ramsay, L., and Coetzee, G. J. R.: Tropospheric ozone climatology over Irene, South Africa, from 1990 to 1994 and 1998 to 2002, *J Geophys Res-Atmos*, 109, Artn D20301 [10.1029/2004jd004793](https://doi.org/10.1029/2004jd004793), 2004.
- Ding, A. J., Wang, T., Thouret, V., Cammas, J. P., and Nedelec, P.: Tropospheric ozone climatology over Beijing: analysis of aircraft data from the MOZAIC program, *Atmos Chem Phys*, 8, 1-13, [Doi 10.5194/Acp-8-1-2008](https://doi.org/10.5194/acp-8-1-2008), 2008.
- 590 Donnell, E. A., Fish, D. J., Dicks, E. M., and Thorpe, A. J.: Mechanisms for pollutant transport between the boundary layer and the free troposphere, *Journal of Geophysical Research: Atmospheres*, 106, 7847-7856, <https://doi.org/10.1029/2000JD900730>, 2001.
- Duncan, B. N., Yoshida, Y., Damon, M. R., Douglass, A. R., and Witte, J. C.: Temperature dependence of factors controlling isoprene emissions, *Geophysical Research Letters*, 36, <https://doi.org/10.1029/2008GL037090>, 2009.
- 595 Fleming, Z. L., Doherty, R. M., von Schneidmesser, E., Malley, C. S., Cooper, O. R., Pinto, J. P., Colette, A., Xu, X. B., Simpson, D., Schultz, M. G., Lefohn, A. S., Hamad, S., Moolla, R., Solberg, S., and Feng, Z. Z.: Tropospheric Ozone Assessment Report: Present-day ozone distribution and trends relevant to human health, *Elementa-Sci Anthropol*, 6, Artn 12 [10.1525/Elementa.273](https://doi.org/10.1525/Elementa.273), 2018.
- 600 Han, S., Yao, Q., Tie, X., Zhang, Y., Zhang, M., Li, P., and Cai, Z.: Analysis of surface and vertical measurements of O₃ and its chemical production in the NCP region, China, *Atmos Environ*, 241, 117759, <https://doi.org/10.1016/j.atmosenv.2020.117759>, 2020.
- He, G. W., Deng, T., Wu, D., Wu, C., Huang, X. F., Li, Z. N., Yin, C. Q., Zou, Y., Song, L., Ouyang, S. S., Tao, L. P., and Zhang, X.: Characteristics of boundary layer ozone and its effect on surface ozone concentration in Shenzhen, China: A case study, *Sci Total Environ*, 791, ARTN 148044 [10.1016/j.scitotenv.2021.148044](https://doi.org/10.1016/j.scitotenv.2021.148044), 2021.
- 605 Inness, A., Ades, M., Agustí-Panareda, A., Barré, J., Benedictow, A., Blechschmidt, A. M., Dominguez, J. J., Engelen, R., Eskes, H., Flemming, J., Huijnen, V., Jones, L., Kipling, Z., Massart, S., Parrington, M., Peuch, V. H., Razinger, M., Remy, S., Schulz, M., and Suttie, M.: The CAMS reanalysis of atmospheric composition, *Atmos. Chem. Phys.*, 19, 3515-3556, [10.5194/acp-19-3515-2019](https://doi.org/10.5194/acp-19-3515-2019), 2019.
- 610 Jaffe, D.: Relationship between Surface and Free Tropospheric Ozone in the Western U.S., *Environ Sci Technol*, 45, 432-438, [10.1021/es1028102](https://doi.org/10.1021/es1028102), 2011.
- Jin, X. M., Fiore, A., Boersma, K. F., De Smedt, I., and Valin, L.: Inferring Changes in Summertime Surface Ozone-NO_x-VOC Chemistry over US Urban Areas from Two Decades of Satellite and Ground-Based Observations, *Environ Sci Technol*, 54, 6518-6529, [10.1021/acs.est.9b07785](https://doi.org/10.1021/acs.est.9b07785), 2020.
- 615 Karl, T., Lamprecht, C., Graus, M., Cede, A., Tiefengraber, M., Vila-Guerau de Arellano, J., Gurarie, D., and Lenschow, D.: High urban NO_x triggers a substantial chemical downward flux of ozone, *Science Advances*, 9, eadd2365, [10.1126/sciadv.add2365](https://doi.org/10.1126/sciadv.add2365), 2023.
- Kaser, L., Patton, E. G., Pfister, G. G., Weinheimer, A. J., Montzka, D. D., Flocke, F., Thompson, A. M., Stauffer, R. M., and Halliday, H. S.: The effect of entrainment through atmospheric boundary layer growth on observed and modeled surface ozone in the Colorado Front Range, *J Geophys Res-Atmos*, 122, 6075-6093, [10.1002/2016JD026245](https://doi.org/10.1002/2016JD026245), 2017.
- 620 Levelt, P. F., Joiner, J., Tamminen, J., Veefkind, J. P., Bhartia, P. K., Zeevaert, D. C. S., Duncan, B. N., Streets, D. G., Eskes, H.,



- van der A, R., McLinden, C., Fioletov, V., Carn, S., de Laat, J., DeLand, M., Marchenko, S., McPeters, R., Ziemke, J., Fu, D. J.,
Liu, X., Pickering, K., Apituley, A., Abad, G. G., Arola, A., Boersma, F., Miller, C. C., Chance, K., de Graaf, M., Hakkarainen,
625 J., Hassinen, S., Ialongo, I., Kleipool, Q., Krotkov, N., Li, C., Lamsal, L., Newman, P., Nowlan, C., Suleiman, R., Tilstra, L. G.,
Torres, O., Wang, H. Q., and Wargan, K.: The Ozone Monitoring Instrument: overview of 14 years in space, *Atmos Chem
Phys*, 18, 5699-5745, 10.5194/acp-18-5699-2018, 2018.
- Li, R. Y., Xu, M. Q., Li, M. C., Chen, Z. Y., Zhao, N., Gao, B. B., and Yao, Q.: Identifying the spatiotemporal variations in
ozone formation regimes across China from 2005 to 2019 based on polynomial simulation and causality analysis, *Atmos
630 Chem Phys*, 21, 15631-15646, 10.5194/acp-21-15631-2021, 2021.
- Liao, Z., Ling, Z., Gao, M., Sun, J., Zhao, W., Ma, P., Quan, J., and Fan, S.: Tropospheric Ozone Variability Over Hong Kong
Based on Recent 20 years (2000–2019) Ozonesonde Observation, *Journal of Geophysical Research: Atmospheres*, 126,
e2020JD033054, <https://doi.org/10.1029/2020JD033054>, 2021.
- Lin, C. H., Wu, Y. L., and Lai, C. H.: Ozone reservoir layers in a coastal environment - a case study in southern Taiwan,
635 *Atmos. Chem. Phys.*, 10, 4439-4452, 10.5194/acp-10-4439-2010, 2010.
- Lin, H., Xing, C., Hong, Q., Liu, C., Ji, X., Liu, T., Lin, J., Lu, C., Tan, W., Li, Q., and Liu, H.: Diagnosis of Ozone Formation
Sensitivities in Different Height Layers via MAX - DOAS Observations in Guangzhou, *Journal of Geophysical Research:
Atmospheres*, 127, 10.1029/2022jd036803, 2022.
- Lu, X., Hong, J. Y., Zhang, L., Cooper, O. R., Schultz, M. G., Xu, X. B., Wang, T., Gao, M., Zhao, Y. H., and Zhang, Y. H.:
640 Severe Surface Ozone Pollution in China: A Global Perspective, *Environ Sci Tech Let*, 5, 487-494,
10.1021/acs.estlett.8b00366, 2018.
- Mills, G., Pleijel, H., Malley, C. S., Sinha, B., Cooper, O. R., Schultz, M. G., Neufeld, H. S., Simpson, D., Sharps, K., Feng, Z.
Z., Gerosa, G., Harmens, H., Kobayashi, K., Saxena, P., Paoletti, E., Sinha, V., and Xu, X. B.: Tropospheric Ozone
Assessment Report: Present-day tropospheric ozone distribution and trends relevant to vegetation, *Elementa-Sci
645 Anthropol*, 6, Artn 47
10.1525/Elementa.302, 2018.
- Monks, P. S., Archibald, A. T., Colette, A., Cooper, O., Coyle, M., Derwent, R., Fowler, D., Granier, C., Law, K. S., Mills, G. E.,
Stevenson, D. S., Tarasova, O., Thouret, V., von Schneidemesser, E., Sommariva, R., Wild, O., and Williams, M. L.:
Tropospheric ozone and its precursors from the urban to the global scale from air quality to short-lived climate forcer,
650 *Atmos Chem Phys*, 15, 8889-8973, 10.5194/acp-15-8889-2015, 2015.
- Neuman, J. A., Trainer, M., Aikin, K. C., Angevine, W. M., Brioude, J., Brown, S. S., de Gouw, J. A., Dube, W. P., Flynn, J. H.,
Graus, M., Holloway, J. S., Lefer, B. L., Nedelec, P., Nowak, J. B., Parrish, D. D., Pollack, I. B., Roberts, J. M., Ryerson, T. B.,
Smit, H., Thouret, V., and Wagner, N. L.: Observations of ozone transport from the free troposphere to the Los Angeles
basin, *Journal of Geophysical Research: Atmospheres*, 117, <https://doi.org/10.1029/2011JD016919>, 2012.
- 655 Ogino, S. Y., Fujiwara, M., Shiotani, M., Hasebe, F., Matsumoto, J., Hoang, T. H. T., and Nguyen, T. T. T.: Ozone variations
over the northern subtropical region revealed by ozonesonde observations in Hanoi, *J Geophys Res-Atmos*, 118,
3245-3257, 10.1002/jgrd.50348, 2013.
- Oltmans, S. J., Johnson, B. J., Harris, J. M., Thompson, A. M., Liu, H. Y., Chan, C. Y., Vomel, H., Fujimoto, T., Brackett, V. G.,
Chang, W. L., Chen, J. P., Kim, J. H., Chan, L. Y., and Chang, H. W.: Tropospheric ozone over the North Pacific from
660 ozonesonde observations, *J Geophys Res-Atmos*, 109, Artn D15s01
10.1029/2003jd003466, 2004.
- Petetin, H., Thouret, V., Fontaine, A., Sauvage, B., Athier, G., Blot, R., Boulanger, D., Cousin, J. M., and Nédélec, P.:
Characterising tropospheric O₃ and CO around Frankfurt over the period 1994–2012 based on MOZAIC–IAGOS aircraft
measurements, *Atmos. Chem. Phys.*, 16, 15147-15163, 10.5194/acp-16-15147-2016, 2016.
- 665 Petetin, H., Sauvage, B., Smit, H. G. J., Gheusi, F., Lohou, F., Blot, R., Clark, H., Athier, G., Boulanger, D., Cousin, J. M.,
Nedelec, P., Neis, P., Rohs, S., and Thouret, V.: A climatological view of the vertical stratification of RH, O₃ and CO within



- the PBL and at the interface with free troposphere as seen by IAGOS aircraft and ozonesondes at northern mid-latitudes over 1994–2016, *Atmos. Chem. Phys.*, 18, 9561–9581, 10.5194/acp-18-9561-2018, 2018.
- Seidel, D. J., Ao, C. O., and Li, K.: Estimating climatological planetary boundary layer heights from radiosonde observations: Comparison of methods and uncertainty analysis, *Journal of Geophysical Research: Atmospheres*, 115, 670 <https://doi.org/10.1029/2009JD013680>, 2010.
- Seinfeld, J. H., and Pandis, S. N.: *Atmospheric Chemistry and Physics from Air Pollution to Climate Change*, third ed. John, W., Sons, Inc., 2016.
- Stauffer, R. M., Thompson, A. M., and Young, G. S.: Tropospheric ozonesonde profiles at long-term US monitoring sites: 1. A climatology based on self-organizing maps, *J Geophys Res-Atmos*, 121, 1320–1339, 10.1002/2015JD023641, 2016.
- 675 Stull, R. B.: *An Introduction to Boundary Layer Meteorology*; Kluwer Academic Publishers, Dordrecht, The Netherlands., 1988.
- Tang, G. Q., Zhu, X. W., Xin, J. Y., Hu, B., Song, T., Sun, Y., Zhang, J. Q., Wang, L. L., Cheng, M. T., Chao, N., Kong, L. B., Li, X., and Wang, Y. S.: Modelling study of boundary-layer ozone over northern China - Part I: Ozone budget in summer, *Atmos Res*, 187, 128–137, 10.1016/j.atmosres.2016.10.017, 2017.
- 680 Trousdell, J. F., Conley, S. A., Post, A., and Faloon, I. C.: Observing entrainment mixing, photochemical ozone production, and regional methane emissions by aircraft using a simple mixed-layer framework, *Atmos. Chem. Phys.*, 16, 15433–15450, 10.5194/acp-16-15433-2016, 2016.
- Wang, P., Yang, Y., Li, H., Chen, L., Dang, R., Xue, D., Li, B., Tang, J., Leung, L. R., and Liao, H.: North China Plain as a hot spot of ozone pollution exacerbated by extreme high temperatures, *Atmos. Chem. Phys.*, 22, 4705–4719, 685 10.5194/acp-22-4705-2022, 2022a.
- Wang, T., Xue, L., Brimblecombe, P., Lam, Y. F., Li, L., and Zhang, L.: Ozone pollution in China: A review of concentrations, meteorological influences, chemical precursors, and effects, *Sci Total Environ*, 575, 1582–1596, <https://doi.org/10.1016/j.scitotenv.2016.10.081>, 2017.
- 690 Wang, T., Xue, L., Feng, Z., Dai, J., Zhang, Y., and Tan, Y.: Ground-level ozone pollution in China: a synthesis of recent findings on influencing factors and impacts, *Environmental Research Letters*, 17, 063003, 10.1088/1748-9326/ac69fe, 2022b.
- Wang, X. Y., and Wang, K. C.: Estimation of atmospheric mixing layer height from radiosonde data, *Atmos. Meas. Tech.*, 7, 1701–1709, 10.5194/amt-7-1701-2014, 2014.
- 695 Williams, A. G., Zahorowski, W., Chambers, S., Griffiths, A., Hacker, J. M., Element, A., and Werczynski, S.: The Vertical Distribution of Radon in Clear and Cloudy Daytime Terrestrial Boundary Layers, *Journal of the Atmospheric Sciences*, 68, 155–174, <https://doi.org/10.1175/2010JAS3576.1>, 2011.
- Wyngaard, J. C., and Brost, R. A.: Top-Down and Bottom-Up Diffusion of a Scalar in the Convective Boundary Layer, *Journal of Atmospheric Sciences*, 41, 102–112, [https://doi.org/10.1175/1520-0469\(1984\)041<0102:TDBUD>2.0.CO;2](https://doi.org/10.1175/1520-0469(1984)041<0102:TDBUD>2.0.CO;2), 700 1984.
- Xu, Z., Chen, H., Guo, J., and Zhang, W.: Contrasting Effect of Soil Moisture on the Daytime Boundary Layer Under Different Thermodynamic Conditions in Summer Over China, *Geophysical Research Letters*, 48, e2020GL090989, <https://doi.org/10.1029/2020GL090989>, 2021.
- 705 Yates, E. L., Johnson, M. S., Iraci, L. T., Ryoo, J. M., Pierce, R. B., Cullis, P. D., Gore, W., Ives, M. A., Johnson, B. J., Leblanc, T., Marrero, J. E., Sterling, C. W., and Tanaka, T.: An Assessment of Ground Level and Free Tropospheric Ozone Over California and Nevada, *Journal of Geophysical Research: Atmospheres*, 122, 10,089–010,102, <https://doi.org/10.1002/2016JD026266>, 2017.
- Yonemura, S., Tsuruta, H., Kawashima, S., Sudo, S., Peng, L. C., Fook, L. S., Johar, Z., and Hayashi, M.: Tropospheric ozone climatology over Peninsular Malaysia from 1992 to 1999, *Journal of Geophysical Research: Atmospheres*, 107, ACH 710 1-1-ACH 1-12, <https://doi.org/10.1029/2001JD000993>, 2002.



- Zhang, J., Li, D., Bian, J., Xuan, Y., Chen, H., Bai, Z., Wan, X., Zheng, X., Xia, X., and Lü, D.: Long-term ozone variability in the vertical structure and integrated column over the North China Plain: results based on ozonesonde and Dobson measurements during 2001–2019, *Environmental Research Letters*, 16, 074053, [10.1088/1748-9326/ac109f](https://doi.org/10.1088/1748-9326/ac109f), 2021.
- 715 Zhao, W., Tang, G. Q., Yu, H., Yang, Y., Wang, Y. H., Wang, L. L., An, J. L., Gao, W. K., Hu, B., Cheng, M. T., An, X. Q., Li, X., and Wang, Y. S.: Evolution of boundary layer ozone in Shijiazhuang, a suburban site on the North China Plain, *J Environ Sci*, 83, 152-160, [10.1016/j.jes.2019.02.016](https://doi.org/10.1016/j.jes.2019.02.016), 2019.
- Zhu, X. W., Ma, Z. Q., Qiu, Y. L., Liu, H., Liu, Q., and Yin, X. M.: An evaluation of the interaction of morning residual layer ozone and mixing layer ozone in rural areas of the North China Plain, *Atmos Res*, 236, ARTN 104788 [10.1016/j.atmosres.2019.104788](https://doi.org/10.1016/j.atmosres.2019.104788), 2020.
- 720